



HAL
open science

Characterization of complex micellar systems by Scattering techniques (SAXS and SANS) and wet-Scanning Transmission Electron Microscopy (wet-STEM)

Jeremy Causse, Cyril Lavaud, Johann Ravaux, Joseph Lautru, Renaud Podor

► **To cite this version:**

Jeremy Causse, Cyril Lavaud, Johann Ravaux, Joseph Lautru, Renaud Podor. Characterization of complex micellar systems by Scattering techniques (SAXS and SANS) and wet-Scanning Transmission Electron Microscopy (wet-STEM). *Colloids and Surfaces A: Physicochemical and Engineering Aspects*, 2024, 682, pp.132928. 10.1016/j.colsurfa.2023.132928 . hal-04487945

HAL Id: hal-04487945

<https://hal.univ-lille.fr/hal-04487945>

Submitted on 4 Mar 2024

HAL is a multi-disciplinary open access archive for the deposit and dissemination of scientific research documents, whether they are published or not. The documents may come from teaching and research institutions in France or abroad, or from public or private research centers.

L'archive ouverte pluridisciplinaire **HAL**, est destinée au dépôt et à la diffusion de documents scientifiques de niveau recherche, publiés ou non, émanant des établissements d'enseignement et de recherche français ou étrangers, des laboratoires publics ou privés.

**Characterization of complex micellar systems by Scattering techniques (SAXS and SANS)
and wet-Scanning Transmission Electron Microscopy (wet-STEM).**

Jeremy Causse, Cyril Lavaud, Johann Ravaux, Joseph Lautru and Renaud Podor*

ICSM, Univ Montpellier, CNRS, CEA, ENSCM, Bagnols-sur-Cèze, France

* Corresponding author

E-mail address: renaud.podor@cea.fr

Full postal address: Institut de Chimie Séparative de Marcoule

ICSM UMR 5257 – CEA / CNRS / UM / ENSCM

Site de Marcoule, Bâtiment 426

BP 17171

F-30207 Bagnols sur Cèze Cedex

FRANCE

Abstract

The morphology of complex micellar assemblies is generally described using indirect methods such as small-angle X-ray scattering (SAXS) or small angle neutron scattering (SANS) that can yield to ambiguous descriptions of the nano-objects when the sample contains multiple structures or completely unknown structures. We herein propose to directly observe the nano-objects formed in P123 pluronic solutions (with and without rare-earth element - REE) using wet-Scanning Transmission Electron Microscopy (wet-STEM) and to compare the results with sample descriptions derived from SAXS and SANS measurements. The results obtained by the different analytical techniques are consistent. Each analytical method provides complementary information that allows the internal structure of the objects, their compositions and their mutual interactions to be described precisely. The main contributions of wet-STEM microscopy are to describe the nano-objects individually and, in particular, to show that the REE content can vary from 1 to 10 from one micelle to another, to observe the dynamics of the nano-objects in the liquid and to prove the co-existence of nano-objects with very different morphologies in the same system.

Keywords: Micelles, SAXS, SANS, Wet-STEM

1. Introduction

Amphiphilic compounds such as surfactants are building blocks of soft matter. They exhibit the property to self-organize into mesoscopic structures that can adopt different morphologies depending on temperature, concentration, or solute addition. These complex micellar systems are usually characterized by indirect methods using light scattering, small-angle X-ray scattering (SAXS) or small angle neutron scattering (SANS) [1,2]. These methods allow the characterization of a large amount of matter. The collected data yield to the average characterization of a wide population of micelles and results in an average view of the system obtained using mathematical models to fit the curves. As the description of the sample results from a mathematical model of the spectra, a major problem can arise when the sample contains multiple structures or completely unknown structures. Thus, both validation of the models and determination of unknown structures can only be achieved by recording images of the individual particles that are in the sample.

Electron microscopy methods such as cryo-TEM [3,4,5] or cryo-SEM [6,7,8] are used to record images of such assemblies for decades. As the sample is quickly frozen before observation, individual objects can be observed under different configurations. These techniques are used to describe the frozen configuration of assemblies but other microscopy techniques could also be implemented to observe these objects directly in the solution, without any sample preparation. Direct observation of 1.5 – 5 μm diameter polyelectrolyte assemblies in the liquid was achieved using Soft X-Ray imaging on the BESSY II synchrotron (Berlin) [9]. Sample preparation is performed at room temperature, as well as the image recording. An image of the polyelectrolyte assembly is recorded within 3 seconds to limit radiation damages due to X-Ray exposure. However, if large particles remains immobile in the solution for 3 seconds, smaller objects will move due to the Brownian motion, and the displacement will be as fast as their size is small. Last, the best image resolution that can be achieved is 20 nm. Thus, this technique is not suitable for the observation of very small (few tens of nanometers) particles or assemblies.

More recently, liquid cells for transmission electron microscopes were developed. Liquids containing the objects to be observed are directly injected into the cells. They are separated from the high vacuum of the TEM column by two 30 nm thick silicon nitride windows. The thickness of the liquid is generally ranging between 0.5 to 2 μm . Among all the possibilities offered by these devices, those cells can be used to observe dynamics [10] and / or growth [11,12,13] of nanoparticles in the solution. This method is also used to observe and describe directly the dynamics [14,15,16] and stability [17] of soft materials [18], including complex micellar systems. However this method remains difficult to implement and requires both the use of a new generation of TEM / STEM microscopes as well as a high level of know-how by the user. Furthermore, the effect of the electron beam, and the associated dose deposited on the sample, can modify the morphology or organization of the objects to be observed [19]. One of the main concerns of the liquid-cell TEM imaging is the effect of the electron beam that can alter or destroy the materials to be observed and / or their environment [18] that can hardly be avoided. The beam damages can sometimes also help for experiments [20].

Scanning electron microscopy (SEM) is also an important technique for the observation of soft materials (including biological samples). As this apparatus works under high vacuum, the specimens must be prepared using fixation and staining methods, and/or a metal coating. Several strategies have been recently developed to undergo these limits, most of them being based upon the use of environmental sample holders, where the sample is fully separated from the microscope chamber. First, in the Wet-SEM device, a drop of solution is deposited in a closed sample holder that isolates wet samples from the high vacuum atmosphere of the SEM chamber [21]. The materials that are present in the solution are directly observed through an electron transparent window using the backscattered electron mode. The interfacial structure of particle-stabilized emulsions was observed with this method [22,23]. Second, a series of adaptations of detectors on a SEM [24], thus of the SEM column geometry [25], allowed Ogura et al. to develop new imaging methodologies which combines secondary electron collection and soft X-ray detection [26,27] that resulted into high resolution images (8 nm) of

wet samples [28] and living cells [29] without radiation defects. In these developments, the sample is contained within a closed environmental cell and the SEM operates under high vacuum conditions.

Bogner et al. have developed a direct method for the characterization of nanometer scale objects dispersed in a solution: the wet-STEM method [30,31]. The principle of this method is to observe directly the particles that are present in a liquid, the thickness of the liquid being sufficiently thin to be transparent to the electron beam. With this method, the liquid is not separated from the chamber of the SEM as a drop of the solution to be observed is directly deposited on a holey carbon grid. The wet-STEM device is implemented in an Environmental Scanning Electron Microscope as it requires both controlling precisely the sample temperature and the water pressure, to equilibrate liquid water of the sample with the water vapor in the chamber of the microscope. This technique allows observing directly nanometer scale solids dispersed in solutions as well as their dynamics [32]. Wet-STEM has also been used to characterize biological materials [33,34], latex-aerogel systems [35], colloidal suspensions, mini-emulsions [30] and soft matter such as micelles [31] and vesicles [36]. The resolution of this technique is in the order of few nanometers [31,33].

The wet-STEM technique remains underused up today, particularly in the field of the characterization of soft matter and micellar systems. The aim of the present study is to perform both wet-STEM and SAXS / SANS methods for the characterization of complex micellar systems in order to validate the ability of wet-STEM for the direct observation of systems that sensitive to the electron beam. Pluronic P123 micelles will be used as a model system. These micelles have been widely studied and described in previous studies. They are very well known for their use as soft template in mesoporous silica synthesis such as SBA-15 [37]. They are also reported to be a part of a separation process allowing recovering of rare-earth elements (REE) from water outflows in a sol-gel method [38]. In this latter case, the addition in aqueous phase of a hydrophobic complexing agent of REE such as bis-(2-ethylhexyl)-phosphoric acid (HDEHP) makes the REE cations migrate from bulk water to P123 micelles. The presence of this REE-HDEHP complex in the micelles therefore modifies the morphology

of the assemblies providing colloids with different shapes and contrasts. Wet-STEM imaging will be used to characterize and describe the different types of assemblies that are formed when modifying the liquid composition. The shape of the nano objects, derived from the SEM images, will be compared with models derived from SANS and SAXS measurements.

2. Material and methods

2.1. Micelle solution preparation

Pluronic P123 solution was purchased from Sigma Aldrich (average molecular weight of 5800) and was used after purification. The lanthanides salts $\text{La}(\text{NO}_3)_3 \cdot 6\text{H}_2\text{O}$ – $\text{Nd}(\text{NO}_3)_3 \cdot 6\text{H}_2\text{O}$ – $\text{Sm}(\text{NO}_3)_3 \cdot 6\text{H}_2\text{O}$ – $\text{Eu}(\text{NO}_3)_3 \cdot 5\text{H}_2\text{O}$ for lanthanum, neodymium, samarium and europium respectively were purchased from Sigma Aldrich with 99.9% of purity and used as received. The bis-(2-ethylhexyl)-phosphoric acid (HDEHP) ligand was purchased from Aldrich and used as received.

The samples were prepared by mixing the components with a milliQ water solution of nitric acid at pH = 4 (0.1 mmol.L⁻¹). The operating temperature was room temperature. All the samples were filtered before measurements with a Versapor® acrylic membrane (cut-off threshold of 1.2 microns). For all the experiments, neodymium was chosen as the reference REE.

The REE-free solution is constituted by water with 1 %wt P123. The sample is called P123-1%. The typical concentrations of each component was set to 1 %wt for P123, 0.14 mM for REE³⁺ and 0.42 mM for HDEHP ligand. In this case, the sample name is P123-1%-REEH. The molar ratio between REE and HDEHP was always kept constant due to the theoretical stoichiometry of REE:HDEHP complex known to be 1:3. 10 and 30 times concentrated systems were also studied, therefore exhibiting concentrations of respectively 10 %wt and 30 %wt for P123, 1.4 mM and 4.2 mM for REE³⁺ and 4.2 mM and 12.6 mM for HDEHP. In this case, the samples are called P123-10%-REEH and P123-30%-REEH

respectively. Table 1 presents the references and compositions of the different samples, as well as the direct and indirect techniques that are used for their characterization.

Sample	Composition	SANS	SAXS	STEM
P123-1%	H ₂ O + 1 %wt P123	X		X
P123-1%-NdH	H ₂ O + 1 %wt P123+ 0.14 mM Nd ³⁺ + 0.42 mM HDEHP	X	X	X
P123-10%-NdH	H ₂ O + 10 %wt P123+ 1.4 mM Nd ³⁺ + 4.2 mM HDEHP		X	
P123-30%-NdH	H ₂ O + 30 %wt P123+ 4.2 mM Nd ³⁺ + 12.6 mM HDEHP		X	X
P123-1%-LaH	H ₂ O + 1 %wt P123+ 0.14 mM La ³⁺ + 0.42 mM HDEHP			X
P123-30%-LaH	H ₂ O + 30 %wt P123+ 4.2 mM La ³⁺ + 12.6 mM HDEHP			X
P123-1%-SmH	H ₂ O + 1 %wt P123+ 0.14 mM Sm ³⁺ + 0.42 mM HDEHP			X
P123-30%-SmH	H ₂ O + 30 %wt P123+ 4.2 mM Sm ³⁺ + 12.6 mM HDEHP			X
P123-1%-EuH	H ₂ O + 1 %wt P123+ 0.14 mM Eu ³⁺ + 0.42 mM HDEHP			X
P123-30%-EuH	H ₂ O + 30 %wt P123+ 4.2 mM Eu ³⁺ + 12.6 mM HDEHP			X

Table 1. References and compositions of the Pluronic samples. Direct and indirect techniques used for their characterization.

2.2. SAXS / SANS

SAXS experiments were carried out with a X-ray energy of 17.45 keV (corresponding to an average wavelength of 0.709 Å⁻¹). Monochromatism is obtained using the Xenocs Fox2D mirror. The 0.8 mm diameter beam is obtained by a two slots collimation. Beam intensities were collected using a 2D plate detector MAR345. The sample to detector distance is 770 mm. This configuration allows covering q values ranging from about 0.1 nm⁻¹ to 30 nm⁻¹. Scattering diagrams were recorded during 3600 s per sample. The image centre was measured precisely by analysing silver behenate, a standard lamellar phase. Samples were analysed in 2 mm diameter glass capillaries. Absolute intensities were considered by normalising the signal with polyethylene. Data were simulated using the SasFit software [39]. Core-shell spheres and cylinders form factors models are given in SI3 while sticky hard sphere structure factor model used to describe interactions between core-shell spheres can be found in the SASFIT guide.

SANS experiments were performed on the PACE beamline at the Léon Brillouin Laboratory (LLB, Orphée Reactor, Gif-sur-Yvette, France). Three spectrometer configurations were chosen to cover the whole q -values range (q being the scattering angle between the incident and the scattered neutron beam): a small angle configuration with a d sample-to-detector distance equal to 5 m and a λ wavelength equal to 12 Å, a medium angle configuration with $d = 5$ m and $\lambda = 6$ Å and finally a wide angle configuration with $d = 1$ m and $\lambda = 6$ Å. All samples for SANS have been prepared in D₂O. Samples were analysed in quartz cells with a thickness of 1 or 2 mm depending on the hydrogen content in the samples. 1mm Quartz cells filled with H₂O were used to normalise the signal so that curves are plotted with absolute intensity. Data processing was done with the PASINET software package [40].

2.3. Wet-STEM

A Quanta 200 Environmental Scanning Electron Microscope (ESEM) FEG (FEI Company, Eindhoven, The Netherlands) equipped with a field electron gun was used to perform the sample observations. The Wet-STEM stage (Scanning Transmission Electron Microscope) is directly attached to the microscope [30]. A schematic description of the wet-STEM stage attached to the ESEM is reported in SI1. The observation conditions are: acceleration voltage = 30 kV, working distance = 7-10 mm, temperature = 2°C, water vapor pressure = 706 Pa. The formation of the thin liquid film is particularly difficult because the sample should not be dried during the pumping sequence. A 20 µl drop of liquid is deposited onto a holey carbon grid. Then, the air that is in the ESEM chamber is progressively replaced by water vapor through a controlled pumping sequence. When the equilibrium is reached between the liquid water (sample) and the water vapor (gas in the chamber), the liquid film is thinned by slightly decreasing the water vapor pressure in the chamber. When an image of the liquid film is obtained in the transmission mode, the water vapor pressure is adjusted to 706Pa, that corresponds to the equilibrium pressure between liquid and gaseous water at T=2°C. During this sequence, the quantity of water that is present in the film is divided by 30 to 100, which yields to a

concentration of the species that are initially present in the liquid. Thus, in order to prevent this concentration effect, the liquid to be observed is diluted by 50 times with pure water prior to the observation. When the sample is ready, STEM images are recorded with a 1 to 10 seconds frame time, on different regions of interest on the sample, in order to show the reproducibility of the observations.

2.4. Monte-Carlo simulations of the electron trajectories

In order to describe the nano-objects of interest, a simplified model of the micelles is adopted. The pluronic P123 molecules have a $C_{290}H_{580}O_{110}$ composition. From SANS measurements [41], each micelle contains 80 pluronic P123 molecules at 20°C/min, with a 1.06 g/cm^3 density. These objects will be considered as perfectly spherical, with a 20 nm diameter.

When neodymium is incorporated in the micelles, the Nd content incorporated in the pluronic P123 micelles determined by SANS measurements remains relatively low and their composition is $80(C_{290}H_{580}O_{110}) + 18Nd$. Neodymium is supposed to be concentrated in the outer shell of the nano-objects. Their density remains equal to 1.06 g/cm^3 and these micelles are spherical with a diameter equal to 20 nm.

For the calculations, we have considered that these objects are positioned at the bottom, at the middle or at the top of the water layer. The thickness of the water layer will be ranging between 50 and 500 nm. For the calculations, the micelles will not be directly put on the carbon support but a 1 nm water layer will be maintained above or below the micelles (depending on their relative position with the carbon layer). Last, the carbon layer of the support is not considered in the model, as the objects can be observed directly through the holes of the holey carbon grid. The water vapor between the objective lens and the water layer is also not considered in the model.

The detector that is used for the transmitted electron collection is a conventional 2 quadrants backscattered electron detector that is inverted and positioned below the sample. The central hole is

shifted outside the detection field of view. The position of the sample is such as the collection angle ranges between 1 and 1190 mRad using the dark field mode. The sample-to-detector distance is 3 mm. The working distance is ranging between 6 and 10 mm. Last, the acceleration voltage is 30 kV.

The electron trajectories and the STEM images are calculated by Monte-Carlo simulation using the Casino software [42,43]. A minimum of 10^6 electron trajectories on each pixel are considered for the image simulations. The computed image resolution is 1 nm. A Weber contrast C will be used to characterize the computed and experimental images. The formula is:

$$C = (n_{\text{nanoobject}} - n_{\text{background}}) / n_{\text{background}},$$

where $n_{\text{nanoobject}}$ is the number of electrons transmitted by the nano-object in the water layer, $n_{\text{background}}$ is the number of electrons transmitted by the water layer of the same thickness.

3. Results

3.1. Characterization of the micellar systems using indirect methods

The diluted systems were first studied with SANS methods. In this case, samples are prepared in D₂O. The contrast between the deuterated solvent and hydrogenated P123 micelles is high enough, allowing measurements even for quite low concentrations. Figure 1 shows the SANS curves obtained for the original P123 micelle on one side, and the effect of the presence of Nd-HDEHP complex on the other side. It is possible to fit the data related to simple micelles with a core-shell model whose parameters are correctly adjusted with the geometrical description of P123 micelles from the literature [41]. Basically, micelles can be considered as a core of hydrophobic PPO chains surrounded by a shell of highly hydrated PEO chains. Fit parameters are listed in Table 2.

	SANS P123-1%	SANS P123-1%-NdH	SAXS P123-10%-NdH	SAXS P123-30%-NdH
--	-----------------	---------------------	----------------------	----------------------

Core-Shell Form Factor	N_{ob} (cm ⁻³)	4.6 10 ¹⁵	4.6 10 ¹⁵	6.1 10 ¹⁵	1.5 10 ¹⁶
	R_c (nm)	6.2	6.2	3.8	4.6
	e_{sh} (nm)	3.0	3.0	5.0	3.8
	$\Delta\rho_c$ (cm ⁻²)	5.5 10 ¹⁰	5.5 10 ¹⁰	2.1 10 ⁹	2.1 10 ⁹
	$\Delta\rho_{sh}$ (cm ⁻²)	1.0 10 ⁹	1.0 10 ⁹	5.1 10 ⁹	5.1 10 ⁹
Core-Shell Structure Factor	R_{HS} (nm)		10.0	11.7	8.2
	τ		0.05	0.098	0.089
	Φ		0.008	0.09	0.2
Cylinder Form Factor	N_{ob} (cm ⁻³)			1.6 10 ¹⁶	2.2 10 ¹⁶
	R_{CYL}			1.6	1.9
	L			500	500

Table 2 : Fit parameters used for SANS measurements in Figure 1. N_{ob} is the number of micelles per volume, R_c is the micelle core radius (R_c), e_{sh} is the micelle shell thickness, $\Delta\rho_c$ is the neutronic scattering contrast of the micelle core and $\Delta\rho_{sh}$ the neutronic scattering contrast of the micelle shell. For the structure factor, R_{HS} is the hard sphere radius, τ the stickiness, and Φ the volume fraction.

The micelle is described as a core-shell structure which diameter reaches 18 nm. The micelle core is bigger than the shell with respective sizes equal to 6.2 nm and 3.0 nm. It is noteworthy that no structure factor is necessary at this step to describe the system. SANS data for the system containing Nd-HDEHP complexes are very similar to the SANS data of the original micelle, with the exception of the small-angle part of the curves. This part of the curves is related to the structure factor of the micelles, i. e. it describes the intermicellar interactions. Assuming micelles as sticky hard spheres with attractive interactions allows describing the global curve by combining this structure factor with the form factor of the simple micelles (Figure 1). Fit parameters for this system are reported in Table 1. The stickiness τ is low, suggesting only a weak aggregation of the micelles. As can be seen from the fit parameters, the presence of Nd complexes in the micelle has only very low impact on the neutron scattering length density. This is because neutrons interact with the nuclei of atoms. As a result, the SANS recorded curves are by far dominated by the contrast between deuterium and hydrogen and the impact of other elements remains weak.

Therefore, the differences observed between the curves related to both systems in Figure 1 are due to a change in the micelles interactions, and this change can only be attributed to the presence of the Nd-HDEHP complex somewhere in the aggregate, even if the lack of contrast does not allow to detect scattered intensity from these complexes. As a consequence we assume that the Nd-HDEHP complexes are located in the outer part of the micelles corona, thus leading to the weak aggregation of micelles.

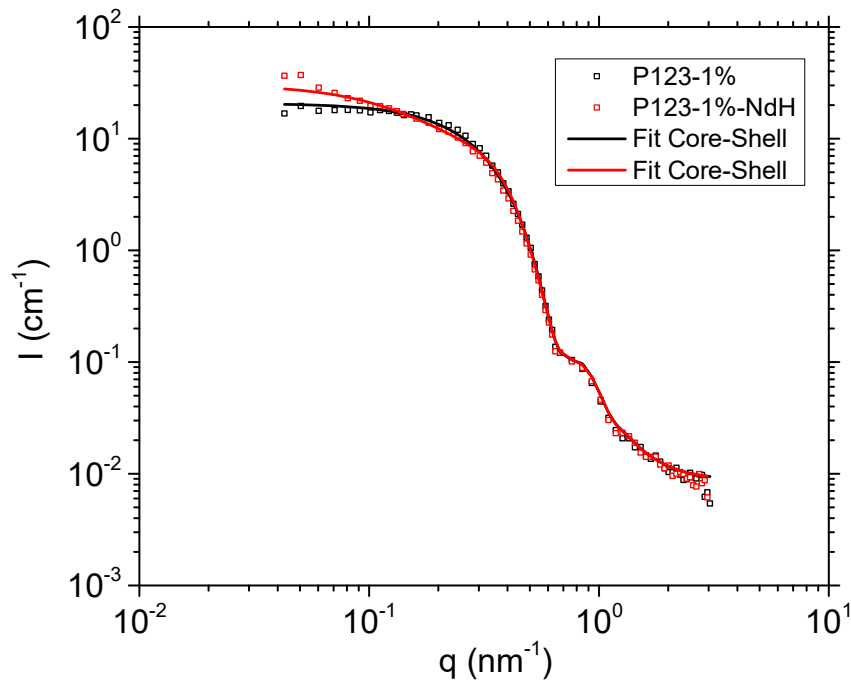


Figure 1. SANS spectra of the P123-1 %wt and P123-1 %wt-NdH diluted systems.

SAXS measurements were also performed to analyze the size and shape changes of the colloids when the concentration of these objects is increased in the liquid. In this case, SAXS technique is convenient because the concentration of soft matter is high enough so that scattered intensity is relevant. Moreover, it is also possible to take into account the presence and the location of Nd-HDEHP complexes due to the fact that X-rays interact with the electrons of the elements. Therefore, Nd presents a high contrast due to its high atomic number. SAXS curves for

concentrated systems with 10 %wt and 30 %wt of P123 in the presence of Nd-HDEHP complexes are reported in Figure 2. Besides, this figure also shows that the system used for SANS measurements with only 1 %wt of P123 is not concentrated enough to record a high quality SAXS curve. This justifies the need to use neutron diffraction to describe the micelles geometry when no structure factor is considered, i.e. for diluted systems. Fitting the curves reported in Figure 2 was difficult due to the several contributions of various form factors needed to adjust correctly the scattered intensity. Consequently, the model used presents many fitting parameters and several solutions can be found out to describe geometrical arrangement of the scatterers. The fitting curves (Figure 2) are based on the contributions of core-shell micelles with sticky interactions just as depicted by SANS measurements on diluted systems, cylinders and a background to take into account the solvent scattering. More than an exact description, this fitting model allows considering the presence of colloids with different shapes in the solution. The limitations of such model is not only due to the high number of fitting parameters but also to the fact that structure factor possibly present in the case of cylinders is very difficult to calculate. Moreover, the length of the cylinders is arbitrary set to 500 nm even if this range of size is out of the q values obtained with the SAXS configuration. This means that another solution of fitting may be possible by increasing the length of the cylinders and decreasing the number of cylinders per volume. Therefore, the model used to fit the data in Figure 2 is complex from a mathematical point of view, but quite simplistic from the possible reality of the solution and those results should be considered with care.

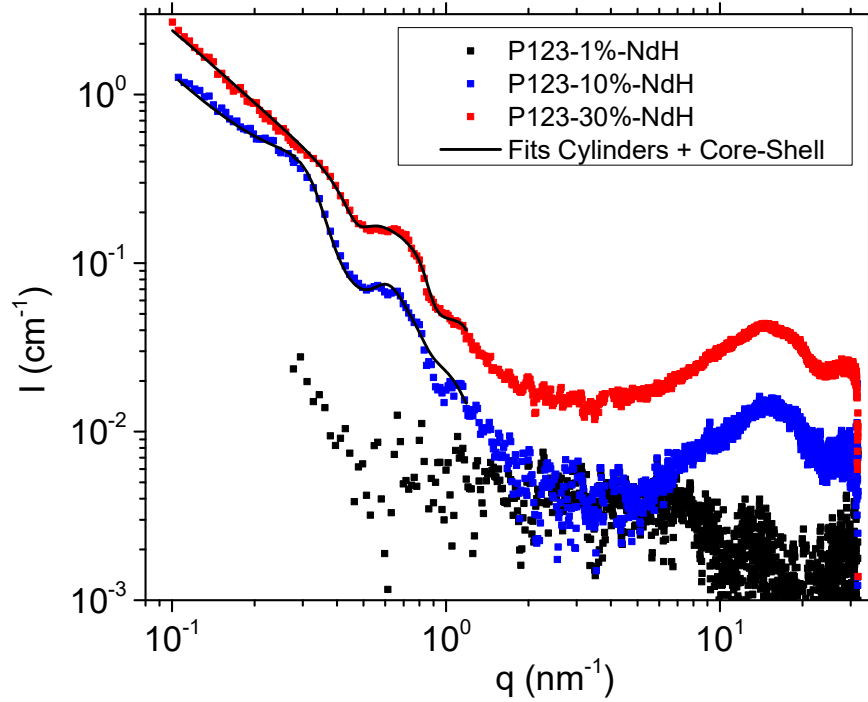


Figure 2. SAXS spectra of the systems, P123-1 %wt-NdH and P123-10 %wt-NdH and P123-30 %wt-NdH

The complexity of these solutions, as well as the lack of confidence in such kind of fits, leads us to consider microscopy measurements, and more particularly wet-STEM analyses to go further and to better depict the shapes and interactions established between the colloids in these liquids.

3.2. Characterization of the micellar systems using wet-STEM

3.2.1. Pluronic micellar system

The pluronic P123-1% micellar system is observed using the wet-STEM sample holder at $T = 2^{\circ}\text{C}$ and $P(\text{H}_2\text{O}) = 706 \text{ Pa}$ (Figure 3a and b). Isolated particles and groups of particles are observed. The isolated particles have a mean diameter equal to $14 (\pm 2) \text{ nm}$. The larger objects are constituted by particles which diameter is close to 14 nm . The isolated particles can group together to form groups of

particles. Larger micelles are also observed. They are probably formed by the coalescence of smaller micelles as described by Parent et al. [15].

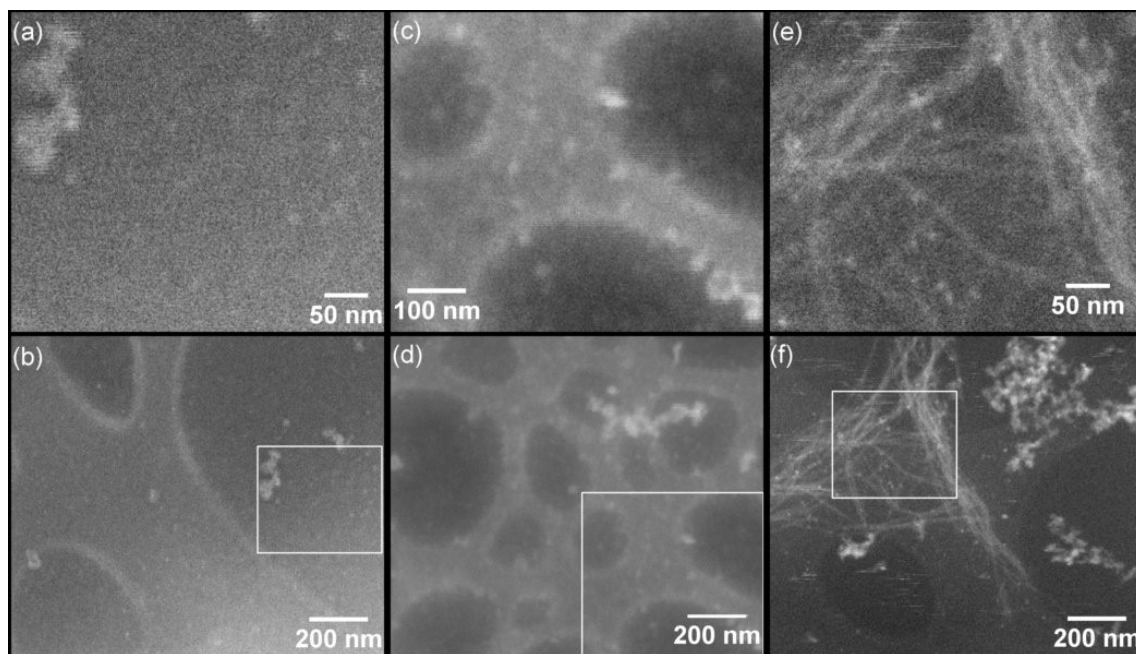


Figure 3. Wet-STEM images recorded at $T = 2^{\circ}\text{C}$ and $P(\text{H}_2\text{O}) = 706 \text{ Pa}$ for a&b) Pluronic P123-1 %wt micelles, c&d) Pluronic P123-1 %wt-NdH micelles, e&f) Pluronic P123-30 %wt-NdH micelles. Inlets in b, d and f represents the zones that are reported in a, c and e. The white squares indicate the magnified areas.

3.2.2. Pluronic micellar system with Nd^{3+}

In the Pluronic P123 solution doped with a low content of neodymium (1.4 mM Nd^{3+} ; P123-30 %wt-NdH), isolated spherical particles are observed using the wet-STEM imaging mode (Figure 3c and d). These micelles are mainly in contact with the boundaries of the holey carbon grid. Some isolated particles are also present in the holes of the holey carbon grid, i.e. dispersed and suspended in the liquid. The contrast of these micelles seems to be more exacerbated than the one of the P123 micelles. Three sets of 25 to 40 diameter measurements were determined from 3 different images recorded during different experiments. The mean diameters obtained for each dataset are $25 (\pm 3) \text{ nm}$, $20 (\pm 4)$

nm and 20 (± 4) nm. Aggregation of micelles is also observed on the images. The aggregates can form circles of micelles. More generally, the aggregates are groups of micelles packed together.

When the concentration of Nd^{3+} in the system is increased to 4.2 mM (P123-30 %wt-NdH), the morphology of the P123-30 %wt-NdH assemblies is strongly modified (Figure 3e and f). The particles that are mainly observed are 13 (± 2) nm diameter nanospheres and micrometer long nanowires. The nanowires are packed together into bundles of nanowires. These structures seem to be in equilibrium with isolated spherical particles (that look like micelles) with a 13 (± 2) nm diameter. These isolated particles are not majority in the mixture. White stripes are also observed in the images. These stripes indicate that the isolated spherical particles are free to move in the liquid water phase. These particles are probably isolated micelles that are not trapped onto the bundles of nanowires. These micelles can also be packed together and form groups of micelles.

3.2.3. Pluronic micellar system with other REEs

When Nd^{3+} is replaced in the solution by another REE (La^{3+} , Sm^{3+} or Eu^{3+}) with a low concentration (P123-1 %wt-REEH), spherical particles are observed (Figure 4a to f). Their average diameters are 29 (± 3), 20 (± 3) and 25 (± 2) nm respectively. These micelles are generally in equilibrium with larger spherical particles that can be groups of micelles or micelles that have fused together to form larger micelles [15].

The increase of the REE content in the solution to 4.2 mM REE^{3+} + HDEHP (P123-30 %wt-REEH), induces a modification of the micelle morphologies, from a spherical shape to a nanowire shape, as already observed with Nd^{3+} (Figure 5). When Nd^{3+} is replaced by La^{3+} or Sm^{3+} , the diameters of the nanowires are close to the one determined for Nd^{3+} , i.e. 13 (± 2) and 15 (± 2) nm respectively. Their lengths are longer than 1 μm . When the REE^{3+} element is Eu^{3+} , the morphology of the micelles looks like cylinders more than nanowires. The diameter of these cylinders is 55 (± 9) nm and their length

remains in the order of 1 μm . By some aspects, the feature of these micelles looks like lamellar micelles.

No spherical micelles still be observable on this pluronic P123-30 %wt-REEH sample.

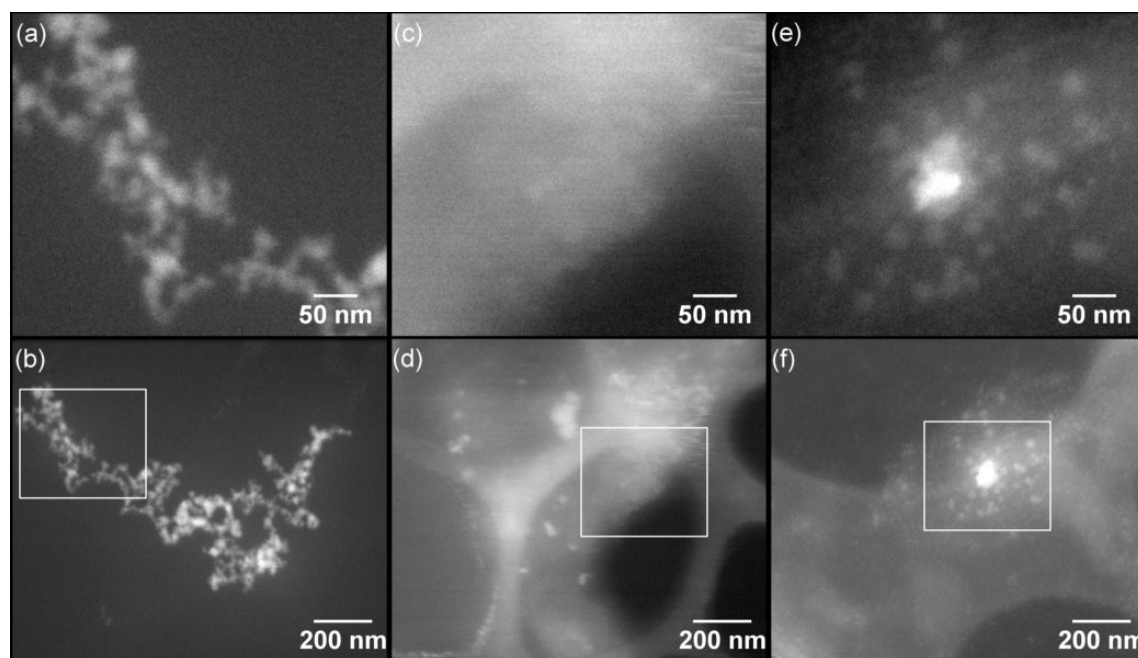


Figure 4. Wet-STEM images recorded at $T = 2^\circ\text{C}$ and $P(\text{H}_2\text{O}) = 706 \text{ Pa}$ for a & b) Pluronic P123-1 %wt-LaH micelles, c & d) Pluronic P123-1 %wt-SmH micelles, e & f) Pluronic P123-1 %wt-EuH micelles. The white squares indicate the areas that are magnified.

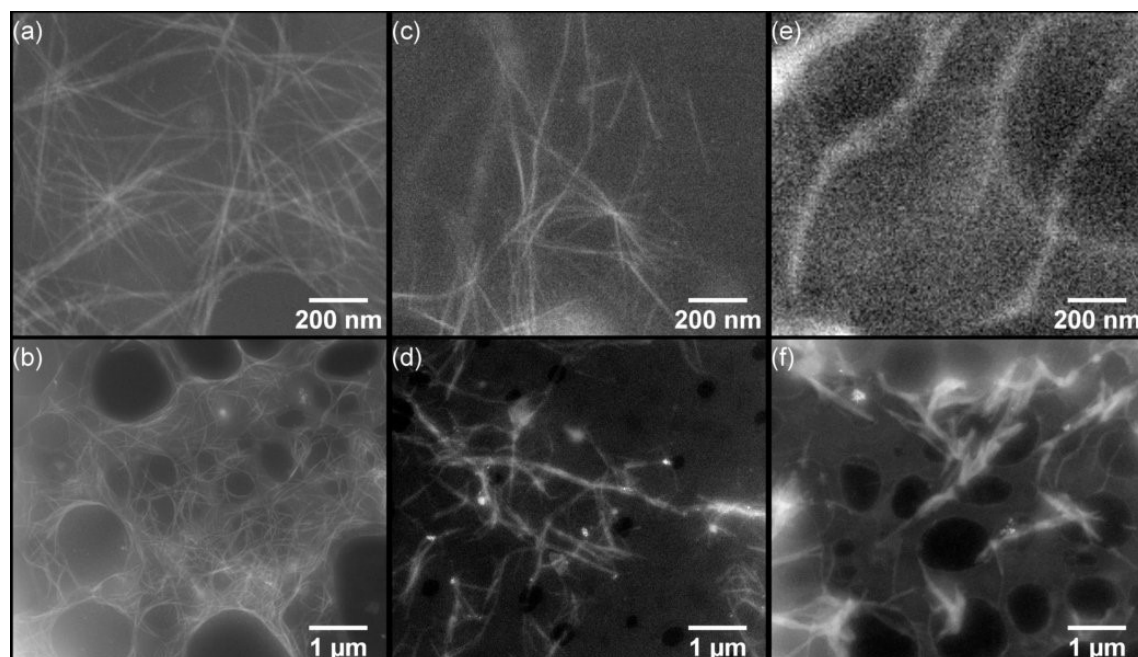


Figure 5. Wet-STEM images recorded at $T = 2^{\circ}\text{C}$ and $P(\text{H}_2\text{O}) = 706 \text{ Pa}$ for a&b) Pluronic P123-30 %wt-LaH micelles, c&d) Pluronic P123-30 %wt-SmH micelles and e&f) Pluronic P123-30 %wt-EuH micelles.

3.2.4. Monte-Carlo simulations of wet-STEM images.

Figure 6a and Figure 6b show Monte-Carlo computed images of P123-1 %wt micelles in a 50 nm and 500 nm water layer (respectively), depending on their relative positions in the water layer. The core-shell model that is used to calculate the P123-1 %wt-NdH micelle images is directly derived from the SANS results. This core-shell structure is not observed in the computed images (see SI2) nor on the real images (Figure 3c), corresponding to the $80(\text{C}_{290}\text{H}_{580}\text{O}_{110}) + 18\text{Nd}$ micelle composition. When the number of rare-earth elements considered in the outer shell of the micelle increases, the outer-shell can be distinguished on the computed images (see SI2), but this corresponds to very high neodymium amounts in the micelles that are far from reality. There is a good agreement between the computed and real images, considering the compositions derived from the SANS analyses. This validates a posteriori the SANS models that have been considered.

Images have been calculated using the Casino software while varying the position of the micelle in the water layer, i.e. considering that it is located at the top, at the middle or at the bottom of the water layer. The computed images are reported in Figure 6a and b and the numerical values of contrasts are gathered in Table 3. No enlargement of the micelle image is observed on the computed images when compared to the theoretical diameter of the micelle. The image resolution is independent of the micelle position in the water layer, as well as it is independent of the thickness of the water layer. Thus, imaging the micelles using the wet-STEM mode should not generate an increase of the apparent size of the micelles on the images and the diameters of the objects can be directly measured from the wet-STEM images.

Figure 6c shows the contrast between the micelles and the water layer, as a function of the water layer thickness. The contrast decreases with increasing the thickness of the water layer, but it remains constant while varying the position of the micelle in the water layer, independently of the thickness of

the water layer. Thus, the contrast of the objects on the wet-STEM images will be as low as the water layer will be thick.

Figure 6d shows the comparison between computed images and real wet-STEM images. The computed images obtained with the Monte-Carlo simulations can be compared with the experimental images recorded using the wet-STEM mode. For the numerical images, the number of transmitted electrons are considered. A profile is obtained by determining the number of transmitted electrons across the diameter of the Monte-Carlo image of the P123-1 %wt micelle in a 50 nm water layer thickness. For the wet-STEM images, the number of transmitted electrons is directly correlated to the grey level of the objects. A grey-level profile is obtained by radially integrating the grey-levels from the center of the wet-STEM image of a micelle to the outer part of the image. Simulated and experimental profiles of 20 nm P123 micelles are reported in Figure 6d. The simulated profiles determined from the simulated images are superimposed with the profiles obtained from the wet-STEM images, indicating that the simulation conditions used to carry out the Monte-Carlo calculations are correct.

The presence of neodymium in the P123-1 %wt-NdH micelle yields to a very limited increase of the contrast values calculated by Monte-Carlo simulation when compared to the P123-1 %wt (REE free) micelles (Figure 6c). Supplementary images were computed while increasing the neodymium content in the micelles (see SI2 for more information). For a fixed water layer thickness, the contrast between the micelle and the water increases with increasing the REE content in the micelle. As a consequence, a variation of the brightness of the objects on the wet-STEM images directly corresponds to a variation of the Nd content in the micelles, for a constant water layer thickness.

According to the results from Monte-Carlo simulations, a limited contrast inversion is observed in the conditions chosen to perform the calculations with the types of micelles studied herein, when the water layer thickness is equal or higher than 750 nm and when the Nd content in the micelle is high. This is in agreement with the data reported by Xiao et al. [44]. However, in the present study, the Monte-Carlo calculations yield to contrast inversion values equal to -0.0002 that are much more lower

and limited than the values reported by Xiao et al. [44] that are as low as -10. This can be due to the difference in the nature of the objects that are considered in each study. Indeed, in the present study, the objects are micelles, mainly constituted by organic matter assemblies with few metallic elements whereas the systems studied by Xiao et al. [44] are gold nanoparticles (10-80 nm radii) dispersed in water. The size and chemical composition of the objects dispersed in water strongly modifies their interaction with the primary electron beam, and as a direct consequence it modifies their contrast. As an example, the contrast of a 20 nm diameter gold nanoparticles in 1000 nm water is approximately equal to 2 while the contrast of 22 nm diameter Nd containing micelles in 1000 nm water is close to 0.

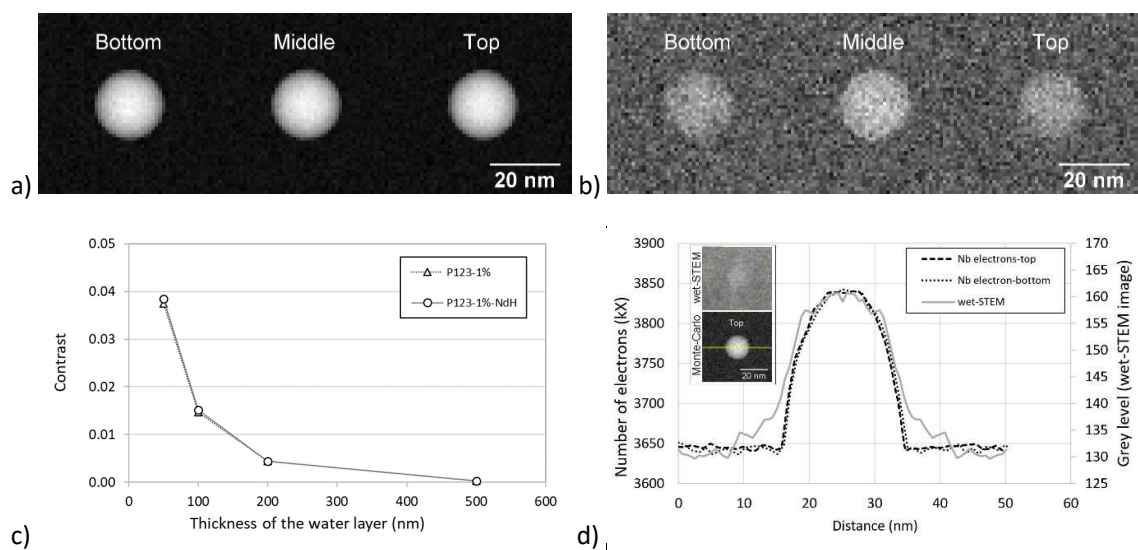


Figure 6. Series of P123-1 %wt micelles with a 20 nm diameter computed images using the Monte-Carlo simulation software in a) a 50 nm water layer. b) a 500 nm water , depending on the position of the micelle in the water layer. c) Contrast values reported as a function of the thickness of the water layer for P123-1 %wt and P123-1 %wt-NdH micelles. Only the results obtained for micelles positioned at the bottom of the water layer are reported. d) Comparison of experimental (wet-STEM) and computed profiles of P123-1 %wt micelles in a 50 nm water layer. The inset images shows the wet-STEM image and the Monte-Carlo image computed with the Casino software.

P123-1%	Thickness (nm)	Bottom	Middle	Top
	50	0.0375	0.0375	0.0374
	100	0.0147	0.0151	0.0147
	200	0.0044	0.0047	0.0044
	500	0.0003	0.0004	0.0003

P123-1%-NdH	Thickness (nm)	Bottom	Middle	Top
	50	0.0385	0.0387	0.0385
	100	0.0152	0.0154	0.0151
	200	0.0045	0.0048	0.0045
	500	0.0003	0.0004	0.0003

Table 3. Contrast values reported for different thicknesses of the water layer for both P123-1 %wt and P123-1 %wt-NdH micellar systems.

4. Discussion

4.1. Presence of water in equilibrium with the nanoobjects

A key point for the use of the wet-STEM mode is to verify that the objects to be observed have always been maintained in a liquid phase. The demonstration of the presence of water on the sample is not enough to ensure that the sample have always been maintained in a liquid phase. Indeed, during the pumping sequence, the sample can have been fully dried and water can later have been condensed on the sample cooled to 2°C. Thus, the only possibility to make sure that the pumping sequence has been operated correctly is to observe the movements of free particles in the liquid.

Evidence of the presence of a liquid phase surrounding the nanoobjects can be seen directly on the wet-STEM images (Figure 7). The lines that appear on the images correspond to micelles that move freely and very fast in the liquid phase (white arrow in Figure 7). As these micelles are free to move in the liquid, this clearly indicates that the drop of solution that has been initially deposited on the carbon grid has not been dried during the pumping sequence. Indeed, if this would have not been the case, all the micelles would have been stuck to the carbon film. Thus, the water film would correspond to condensed water and no micelles would be free to move in the liquid phase (nor remain stable in pure water). Limited movements of the nanowires (and bundles of nanowires) are also observed on the

image series. These movements indicate that the nanowires are not stuck to the carbon membrane but they are also free to move in the liquid layer.

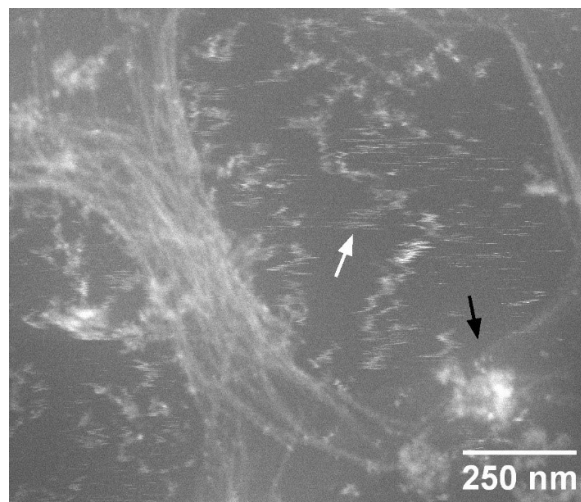


Figure 7. Wet-STEM image of bundles of nanowires in equilibrium with micelles ($T = 2^{\circ}\text{C}$, $P = 690 \text{ Pa}$ H_2O) in the P123-30 %wt-NdH sample (30 %wt P123 + 4.2 mM Nd^{3+} + HDEHP 12.6 mM).

4.2. Evidence for equilibrium between the different morphologies

The direct observation of these movements clearly indicates that micelles and nanowires remain present in the solution with which they are in equilibrium. As SAXS or SANS methods can only allow the characterization of an average population of nano-objects, the equilibrium between several morphologies (and in some particular cases the transformation of the morphology of nano-objects [15]) is clearly evidenced by microscopy techniques such as wet-STEM imaging.

In the particular case of the P123-30 %wt-NdH sample, the results of the curve fitting yields to several possibilities to describe the objects that are in the liquid. Thus, only direct imaging can provide a fine description of these nano-objects.

4.3. Contrasts, position of the nano-objects, thickness of the water layer

When considering the nanowires, the bundles of nanowires shown by a black arrow in Figure 7 go below the plane formed by the group of micelles. This corresponds to a decrease of the contrast of the bundle of nanowires when the thickness of water above the bundle of nanowires increases. The other part of the same bundle of nanowires seems to reappear on the image on the other side of the group of micelles. From this observation, one can conclude that the bundles of nanowires tend to float at the surface of the liquid. In this region of the sample, the water layer is probably relatively thick. The micelles are free to move and the nanowires seem to be immobile because they form bundles that limit their movements. In the P123-30 %wt-NdH sample, the neodymium content in the nano-objects is higher than in the P123-1 %wt-NdH sample. Thus, as the nano-objects are relatively free to move and as their contrast with the liquid phase remains relatively high (see SI2), the thickness of the water layer is probably equal to or higher than a few hundreds of nanometers.

The possibility to record images of P123-1 %wt or P123-1 %wt-NdH micelles using the wet-STEM mode implies that these objects are stuck to the carbon layer. If not, their movements in the liquid phase, due to the Brownian motion, would make it impossible to see the micelles. Furthermore, the numerical images obtained by Monte-Carlo simulation of the P123-1 %wt and P123-1 %wt-NdH micelles exhibit a sufficiently high contrast only when the thickness of the water layer is very low (from 50 to 100 nm). Thus, when observing these samples using the wet-STEM mode, the thickness of the water layer in the region of interest is probably lower than 100 nm (see Table 3).

4.4. Morphology of the nano-objects

The self-assembled nano-objects formed in the liquid phase present morphologies that are identified similarly by indirect methods (SAXS and SANS) and by microscopy (wet-STEM imaging). The spherical shape is the characteristic morphology attributed to these P123-1 %wt self-assemblies from the scattering spectra, and their diameter is found to be equal to 18.4 nm (at room temperature). SAXS

and SANS data generally yield to a diameter of the pluronic P123 micelles ranging between 16 and 18.4 nm [45,46] in water at $T = 20^{\circ}\text{C}$. From the data obtained by Manet et al. [41] at $T = 20^{\circ}\text{C}$ and 40°C , the diameter of the P123 micelles can be linearly extrapolated to 2°C to 17.8 nm. The pluronic P123-1 %wt micelles are also characterized by a spherical shape and a mean diameter equal to $14 (\pm 2)$ nm by wet-STEM (at $T = 2^{\circ}\text{C}$). Both values are in good agreement and consistent with data previously reported in the literature. The lower diameter of the micelles measured by electron microscopy can be attributed to the variability of the micelle sizes, as observed on the wet-STEM image of the P123 micelles reported in Figure 3a. Indeed, the Monte-Carlo simulations yielded to the conclusion that the contrast of the nano-objects does not vary with the thickness of the water layer. Thus, the diameter of the micelles are not underestimated or overestimated by this technique.

4.5. Composition of the P123 + Nd micelles

An attempt to represent a 3-dimensional view of the P123 micelles containing Nd^{3+} , where the height value is correlated with the grey level of the pixels, show that the micelles are not deformed and homogeneous in size (Figure 8). However, not all the micelles that are represented have the same apparent height. Indeed, the contrast of the micelles is directly correlated to the Nd^{3+} content in the micelles, as shown by the Monte-Carlo simulations (see SI2), considering a constant thickness of the water layer. Thus, if the neodymium content in the micelle varies, the contrast of the micelle will also vary and the apparent height will be as high as the Nd content in the micelle is high. Such a representation indicates that not all the micelles contain the same amount of Nd^{3+} in their structure. If one considers the contrast values reported on Figure 6c, the neodymium content in the micelles probably varies almost from 1 to 10. This local information relative to unique micelles can only be brought by electron microscopy, while global techniques such as SAXS and SANS provide a general information (18 atoms of Nd in the micelles) concerning a wide population of objects. With the wet-

STEM images reported in this work, new information on the variability of the composition of the micelles are accessible.

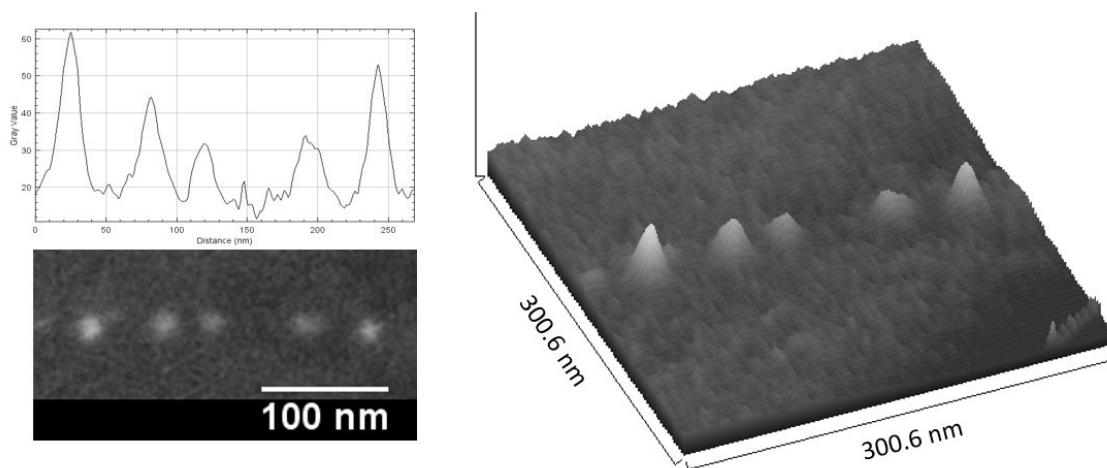


Figure 8. 3-dimensional view of the P123-1 %wt-NdH micelles in the solution. The z direction corresponds to the grey level of the pixels and it is reported as an arbitrary unit.

4.6. Composition of the P123-x %wt-REEH micelles

Low concentration systems (x = 1)

When neodymium is present in the solution with the P123 micelles, this element yields to a growth of the size of the P123-1 %wt-REEH micelles that can be measured by wet-STEM and SANS measurements. Results obtained with both techniques confirm that the morphology of the self-assemblies is a sphere. The diameters of the Nd-containing micelles are 20-25 nm and 18.4 nm (for wet-STEM and SAXS/SANS respectively). These results are consistent. The increase of the micelle size with the incorporation of Nd^{3+} observed by wet-STEM is consistent with data reported in the literature. The same behavior is reported for the incorporation of iron into micelles made of acidic bacterial recombinant protein (MamC) where the average diameter of the micelles increases with the incorporation of the metallic element [47,48]. Parallel to the metal doping of the micelle, an increase of the contrast of the micelles that contains metallic elements is also reported. In the present study, an increase of the contrast between the micelles and the surrounding liquid is also observed (Figure

3c and d), indicating that the neodymium ions are trapped into the micelles. This observation is confirmed by the results of the Monte-Carlo simulations. Indeed, the contrast values increase when the quantity of neodymium contained in the micelles increases (Table 3).

The sizes of the micelles were measured for different REE and the variation of the mean diameter of the micelles are reported in Figure 9 as a function of the ionic radii of the REE³⁺ ion in water. A constant decrease of the diameter of the micelles with the ionic radius of the REE³⁺ ions is evidenced. This trend is not verified for europium. Indeed, this element can exhibit two oxidation states, Eu²⁺ and Eu³⁺, the Eu²⁺ ionic radius being 14% larger than the Eu³⁺ ionic radius. Thus, if a part of the europium is incorporated in the micelles in the form of Eu²⁺ ions, the average mean ionic radius of the europium ions is higher than 0.106 nm (ionic radius of Eu³⁺), and the dot corresponding to europium on Figure 9 should be shifted to the higher ionic radius values to verify the trend. From this assumption, it can be derived that 25 to 30% of europium in the micelles is present in the form of Eu²⁺ ions.

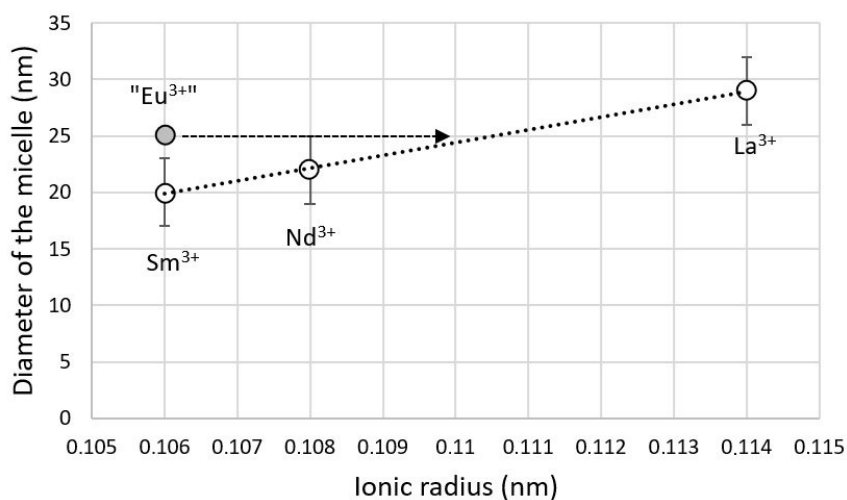


Figure 9. Variation of the diameter of the P123-1 %wt-REEH micelle as a function of the ionic radius of the REE³⁺.

High concentrated systems (x = 30)

When the P123 and REE³⁺ contents in the solution is increased (P123-30 %wt-REEH samples), the general trend that is observed is a modification of the morphology of the nano-objects that are formed: 1 μm long nanowires packed into bundles are in equilibrium with 15 nm diameter nanospheres. Such bundles of nanowires has not been reported but this morphology is close to the wormlike micelles described by Guo et al. [49] and observed by conventional TEM and AFM by Petrov et al. [50]. In the work by Petrov et al., the diameters of the P123 wormlike micelles are close to 10-12 nm when measured on the reported TEM image and 20-25 nm when measured on the reported AFM image. These values are in the same order of magnitude than the diameter of the nanowires measured herein. Furthermore, these wormlike micelles are much more tortuous than the nanowires observed in the present study. This could be attributed to the drying of these structures when deposited on the TEM grid or mica surface that can modify their morphologies. Contrarily, the bundles of nanowires reported herein were never dried and they correspond to the raw organization of the micelles in the liquid. In the present work, no direct correlation is found between the diameter and / or length of the nanowires that are formed and the ionic radius of the REE³⁺ element considered.

In the particular case of a liquid that contains a high concentration of europium and HDEHP, the morphology of the micelles is by some aspects more lamellar than in the form of nanowires. A transition from wormlike micelles to lamellar micelles is already reported to occur with the increase of the C14-diol content in Pluronic P105-water mixtures [49].

The P123-30 %wt-REEH samples (that contain a high content of REE³⁺) cannot be described accurately using indirect methods such as SAXS. Indeed, the spectra corresponding to these liquids can be adjusted considering a combination of different objects (spherical and cylindrical objects) that are in equilibrium in the liquid phase. However, the adjustment of the computational parameters can yield to several solutions and the system cannot be accurately described from SAXS spectra. Thus, in this case, only a direct observation of the liquid – and more particularly of the nanoobjects that are present

in the liquid – provides a clear information on the morphology of the micelles. In this particular case, almost two different morphologies of micelles are in equilibrium with the liquid.

5. Conclusions

The systems chosen for this study, i.e. P123 pluronic solution with rare-earth elements, were selected because they form nano-objects with varying sizes and shapes depending on the preparation conditions. They are used as a model systems for comparing the results obtained with different experimental techniques, whether direct (wet-STEM) or indirect (SANS or SAXS) methods. The objective is to show the contribution of wet-STEM microscopy to the characterization of complex micellar systems that are difficult to describe by indirect methods. Here, this is particularly true due to the change in shape and interactions of the micelles when REEs turn amphiphilic under specific organic ligand complexation.

The results obtained show that the wet-STEM mode attached with the environmental scanning electron microscope (ESEM) makes it possible to acquire information on nanometric objects that are unstable outside the liquid phase with which they are in equilibrium, and without any particular preparation. It is well known that surfactant solutions, in particular Pluronics, can undergo from spherical to wormlike micelles when amphiphilic compounds are accommodated in the surfactant assemblies, either indirect methods such as rheology, SANS, SAXS or direct method in dry state (cryo-TEM) are used to prove this structural change [49, 50]. The present study allows the combination of both indirect and direct methods to give a more precise description of the complex objects rising in solution upon the addition of an organic ligand. These results provide particularly important information for the fine and precise characterization of micellar nano-objects on three particular points.

Firstly, this technique allows the morphological description of individual nano-objects with a minimum dimension of 10 nm and provides local information on their size and shape. In addition, it provides indirect access (through the contrast of the objects) to their compositional variations. The results show that the REE content can vary from 1 to 10 from one micelle to another. However, the REE content fluctuations within the objects (between the core and the corona which are determined by SANS or SAXS analyses) are too low to be observable by the wet-STEM method. Moreover, the recorded images of the nano-objects are at the resolution limit of the technique and would probably not allow such contrasts to be highlighted.

Secondly, complex systems where several morphologies of nano-objects coexist in solution have been evidenced. Here, spherical micelles are in equilibrium with bundles of nanowires. In this case, such systems cannot be described by indirect methods. Indeed, the models used to simulate the experimental SANS and/or SAXS curves lead to several solutions, and it is rather impossible to distinguish which one gives the best descriptions of the reality.

Third, nano-objects are observed directly in the liquid phase with which they are in equilibrium, without the need for any particular preparation that could modify their morphology and that freezes the system in a single particular configuration [5, 8]. Wet-STEM imaging allows observing the movements of the nano-objects in the liquid and eventually their reorganizations. We have shown that spherical micelles whose diameter is about a few tens of nanometers are very mobile and that they can only be correctly observed if they are stuck on the carbon support of the TEM grid. When observing larger objects (here bundles of nanowires), their mobility decreases. This decrease in mobility is probably related to their size and to the interactions that a nanowire has with the surrounding objects. It can also be linked to the limited thickness of the liquid film (a few hundred nanometers thick).

Through the observation of unusual bundles of nanowires, this work clearly illustrates the possibilities offered by the wet-STEM microscopy in the study of complex micellar systems, particularly when the systems contains several morphologies of micelles. Furthermore, as the wet-STEM stage

allows controlling precisely the sample temperature in the -10 – 22 °C temperature range, it could be used to observe directly the temperature effect on the native systems. This study paves the way for further works that will be performed in order to characterize the dynamics of the solutions, as well as the thermal stability domain of the assemblies.

Financial support: The authors thank the French Commissariat à l’Energie Atomique et aux Energies Alternatives (CEA) for financial support.

References

- [1] J.P. Patterson, M.P. Robin, C. Chassenieux, O. Colombani, R.K. O'Reilly, The analysis of solution self-assembled polymeric nanomaterials, *Chem. Soc. Rev.* 43 (2014) 2412–2425.
- [2] E.G. Kelley, R.P. Murphy, J.E. Seppala, T.P. Smart, S.D. Hann, M.O. Sullivan, T.H. Epps, Size Evolution of Highly Amphiphilic Macromolecular Solution Assemblies via a Distinct Bimodal Pathway, *Nat. Commun.* 5 (2014) 1–10.
- [3] P.K. Vinson, *Cryo-electron microscopy of microstructures in complex liquids*; University Microfilms International: Ann Arbor, MI, 1990.
- [4] M. Goldraich, Y. Talmon, Direct-imaging cryo-transmission electron microscopy in the study of colloids and polymer solutions. Amphiphilic block copolymers. Self-assembly and applications. (2000) 253-280.
- [5] Y.-Y. Won, A.K. Brannan, H.T. Davis, F.S. Bates, Cryogenic transmission electron microscopy (Cryo-TEM) of micelles and vesicles formed in water by poly(ethylene oxide)-based block copolymers, *J. Phys. Chem. B* 106 (2002) 3354–3364.
- [6] J. Luo, Z.W. Wang, F. Wang, H. Zhang, J. Lu, H. Y. Guo, F. Z. Ren, Cryo-SEM images of native milk fat globule indicate small casein micelles are constituents of the membrane, *RSC Adv.* 4 (2014) 48963.
- [7] C. Lang, J.A. LaNasa, N. Utomo, Y. Xu, M.J. Nelson, W. Song, M.A. Hickner, R.H. Colby, M. Kumar, R.J. Hickey, Solvent-non-solvent rapid-injection for preparing nanostructured materials from micelles to hydrogels. *Nat. Commun.* 10 (2019) 3855.
- [8] M. Placzek, M. Kosela, Microscopic methods in analysis of submicron phospholipid dispersions. *Acta Pharm.* 66 (2016) 1–22.
- [9] K. Kohler, C. Déjugnat, M. Dubois, T. Zemb, G.B. Sukhorukov, P. Guttman, H. Mohwald, Soft X-ray microscopy to characterize polyelectrolyte assemblies, *J. Phys. Chem. B* 111 (2007) 8388-8393.
- [10] T.A. J. Welling, S. Sadighikia, K. Watanabe, Al. Grau-Carbonell, M. Bransen, D. Nagao, A. van Blaaderen, M. A. van Huis, Observation of undamped 3D brownian motion of nanoparticles using liquid-cell scanning transmission electron microscopy, *Part. Part. Syst. Charact.* 37 (2020) 2000003.
- [11] T.J. Woehl, J. E Evans, I. Arslan, W.D. Ristenpart, N. D. Browning, Direct in situ determination of the mechanisms controlling nanoparticle nucleation and growth, *ACS Nano* 6 (2012) 8599–8610.
- [12] J.P. Patterson, P. Abellan, M.S. Denny, C. Park, N.D. Browning, S.M. Cohen, J.E. Evans, N.C. Gianneschi, Observing the growth of metal–organic frameworks by in situ liquid cell transmission electron microscopy, *J. Am. Chem. Soc.* 137 (2015) 7322–7328.

-
- [13] D. Alloyeau, W. Dachraoui, Y. Javed, H. Belkahla, G. Wang, H. Lecoq, S. Ammar, O. Ersen, A. Wisnet, F. Gazeau, C. Ricolleau, Unravelling Kinetic and Thermodynamic Effects on the Growth of Gold Nanoplates by Liquid Transmission Electron Microscopy, *Nano Lett.* 15 (2015) 2574–2581.
- [14] M.T. Proetto, A.M. Rush, M.-P. Chien, P. Abellan Baeza, J.P. Patterson, M.P. Thompson, N.H. Olson, C.E. Moore, A.L. Rheingold, C. Andolina, J. Millstone, S.B. Howell, N.D. Browning, J.E. Evans, N.C. Gianneschi, Dynamics of soft nanomaterials captured by transmission electron microscopy in liquid water, *J. Am. Chem. Soc.* 136 (2014) 1162–1165.
- [15] L.R. Parent, E. Bakalis, A. Ramírez-Hernández, J.K. Kammeyer, C. Park, J. de Pablo, F. Zerbetto, J.P. Patterson, N.C. Gianneschi, Directly observing micelle fusion and growth in solution by liquid cell transmission electron microscopy, *J. Am. Chem. Soc.* 139 (2017) 17140-17151.
- [16] M.A. Touve, C.A. Figg, D.B. Wright, C. Park, J. Cantlon, B.S. Sumerlin, N.C. Gianneschi, Polymerization-induced self-assembly of micelles observed by liquid cell transmission electron microscopy, *ACS Cent. Sci.* 4 (2018) 543–547.
- [17] J.T. Early, K.G. Yager, T.P. Lodge, Direct observation of micelle fragmentation via in situ liquid phase transmission electron microscopy, *ACS Macro Lett.* 9 (2020) 756–761.
- [18] K. He, T. Shokuhfar, R. Shahbazian-Yassar, Imaging of soft materials using in situ liquid-cell transmission electron microscopy, *J. Phys.: Condens. Matter* 31 (2019) 103001.
- [19] T.J. Woehl, K.L. Jungjohann, J.E. Evans, I. Arslan, W.D. Ristenpart, N.D. Browning, Experimental procedures to mitigate electron beam induced artifacts during in situ fluid imaging of nanomaterials. *Ultramicroscopy* 127 (2013) 53–63.
- [20] S.Pu, C. Gong, A.W. Robertson, Liquid cell transmission electron microscopy and its applications. *R. Soc. open sci.* 7 (2020) 191204.
- [21] V. Behar, A. Nechushtan, Y. Kliger, O. Gileadi, D. Sprinzak, O. Zik, Y. Karni, Methods for SEM inspection of fluid containing samples. Patent No.: US 7,230,242 B2. Jun. 12, 2007
- [22] A.K. F. Dyab, V.N. Paunov, Particle stabilised emulsions studied by WETSEM technique, *Soft Matter* 6 (2010) 2613–2615.
- [23] M. Mayer, D. Dedovet, Y. Guari, J. Larionova, J. Long, J. Causse. Synthesis of poly(diallyldimethylammonium) capped copper hexacyanoferrate (CuHCF) nanoparticles: An efficient stabiliser for Pickering emulsions, *J. Colloid Interface Sci.* 505 (2017) 364-372.
- [24] T. Ogura, A high contrast method of unstained biological samples under a thin carbon film by scanning electron microscopy. *Biochem. Biophys. Res. Commun.* 377 (2008) 79–84.
- [25] T. Ogura, Direct observation of unstained biological specimens in water by the frequency transmission electric-field method using SEM. *PLoS ONE* 9 (2014) e92780.

-
- [26] T. Ogura, Direct observation of unstained wet biological samples by scanning-electron generation X-ray microscopy. *Biochem. Biophys. Res. Commun.* 391 (2010) 198–202.
- [27] T. Ogura, Direct observation of the inner structure of unstained atmospheric cells by low-energy electrons, *Meas. Sci. Technol.* 23 (2012) 085402.
- [28] T. Ogura, High-contrast Observation of unstained proteins and viruses by scanning electron microscopy, *PLoS ONE* 7 (2012) e46904.
- [29] T. Okada, T. Ogura, High-resolution imaging of living mammalian cells bound by nanobeads-connected antibodies in a medium using scanning electron assisted dielectric microscopy, *Scientific Reports* 7 (2017) 43025.
- [30] A. Bogner, G. Thollet, D. Basset, P.-H. Jouneau, C. Gauthier, Wet STEM: A new development in environmental SEM for imaging nano-objects included in a liquid phase, *Ultramicroscopy* 104 (2005) 290-301.
- [31] A. Bogner, P.-H. Jouneau, G. Thollet, D. Basset, C. Gauthier, A history of scanning electron microscopy developments: Towards “wet-STEM” imaging, *Micron* 38 (2007) 390-401.
- [32] J.-M. Teulon, C. Godon, L. Chantalat, C. Moriscot, J. Cambedouzou, M. Odorico, J. Ravaux, R. Podor, A. Gerdil, A. Habert, N. Herlin-Boime, S.-W. Chen, J.-L. Pellequer, On the operational aspects of measuring nanoparticle sizes, *Nanomaterials* 9 (2019) 18.
- [33] D.B. Peckys, N. de Jonge, Gold nanoparticle uptake in whole cells in liquid examined by environmental scanning electron microscopy. *Microsc. Microanal.* 20 (2014) 189–197.
- [34] D.B. Peckys, U. Korf, N. de Jonge, Local variations of HER2 dimerization in breast cancer cells discovered by correlative fluorescence and liquid electron microscopy, *Sci. Adv.* 1 (2015) e1500165.
- [35] A. Perret, G. Foray, K. Masenelli-Varlot, E. Maire, B. Yrieix, Study of the surfactant role in latex–aerogel systems by scanning transmission electron microscopy on aqueous suspensions, *J. Microsc.* 269 (2018) 3-13.
- [36] G. Béalle, L. Lartigue, C. Wilhelm, J. Ravaux, F. Gazeau, R. Podor, D. Carrière, C. Ménager, Surface decoration of cationic vesicles with superparamagnetic iron oxide nanoparticles: a model system for triggered release under moderate temperature conditions, *Phys. Chem. Chem. Phys.* 16 (2014) 4077-4081.
- [37] D. Zhao, J. Feng, Q. Huo, N. Melosh, G.H. Fredrickson, B.F. Chmelka, G.D. Stucky, Triblock copolymer syntheses of mesoporous silica with periodic 50 to 300 angstrom pores, *Science* 279 (1998) 548-552.
- [38] C. Lavaud, F. Goettmann, A. Grandjean, J. Causse, Simultaneous lanthanides and surfactants micelles removal from aqueous outflows by complexation and sol-gel chemistry, *Sep. Purif. Technol.* 145 (2015) 17-23.

-
- [39] I. Breßler, J. Kohlbrecher, A.F. Thünemann, SASfit: a tool for small-angle scattering data analysis using a library of analytical expressions, *J. Appl. Crystallogr.* 48 (2005) 1587-1598.
- [40] PASINET: data treatment software for SANS spectrometers at LLB. Free software available at: <https://www-llb.cea.fr/Phocea/Page/index.php?id=84>
- [41] S. Manet, A. Lecchi, M. Imperor-Clerc, V. Zholobenko, D. Durand, C.L.P. Oliveira, J. Skov Pedersen, I. Grillo, F. Meneau, C. Rochas, Structure of Micelles of a Nonionic Block Copolymer Determined by SANS and SAXS, *J. Phys. Chem. B* 115 (2011) 11318–11329.
- [42] D.Drouin, A.R. Couture, D. Joly, X. Tastet, V. Aimez, R. Gauvin, CASINO V2.42 2 A fast and easy-to-use modeling tool for scanning electron microscopy and microanalysis users, *Scanning* 29 (2007) 922101.
- [43] R.J. Needs, M.D. Towler, N.D. Drummond, P. Lopez Rios, J. R. Trail, Variational and diffusion quantum Monte Carlo calculations with the CASINO code, *J. Chem. Phys.* 152 (2020) 154106.
- [44] J. Xiao, G. Foray, K. Masenelli-Varlot, Analysis of liquid suspensions using scanning electron microscopy in transmission: estimation of the water film thickness using Monte–Carlo simulations, *J. Microsc.* 269 (2018) 151-160.
- [45] S.S. Soni, G. Brotons, M. Bellour, T. Narayanan, A. Gibaud, Quantitative SAXS analysis of the P123/water/ethanol ternary phase diagram, *J. Phys. Chem. B* 110 (2006) 15157-15165.
- [46] V. Patel, J. Dey, R. Ganguly, S. Kumar, S. Nath, V.K. Aswal, P. Bahadur, Solubilization of hydrophobic alcohols in aqueous Pluronic solutions: investigating the role of dehydration of the micellar core in tuning the restructuring and growth of Pluronic micelles, *Soft Matter* 9 (2013) 7583-7591.
- [47] S. Kashyap, T. Woehl, C. Valverde-Tercedor, M. Sánchez-Quesada, C. Jiménez López, T. Prozorov, Visualization of iron-binding micelles in acidic recombinant biomineralization protein, MamC, *J. Nanomater.* (2014) 320124.
- [48] S. Kashyap, T.J. Woehl, X. Liu, S.K. Mallapragada, T. Prozorov, Nucleation of iron oxide nanoparticles mediated by Mms6 Protein in situ, *ACS Nano* 8 (2014) 9097–9106.
- [49] L. Guo, R.H. Colby, M.Y. Lin, G.P. Dado, Micellar structure changes in aqueous mixtures of nonionic surfactants, *J. Rheol.* 45 (2001) 1223-1243.
- [50] P. Petrov, J. Yuan, K. Yoncheva, A.H.E. Muller, C.B. Tsvetanov, Wormlike morphology formation and stabilization of “Pluronic P123” micelles by solubilization of pentaerythritol tetraacrylate, *J. Phys. Chem. B* 112 (2008) 8879–8883.